Boundary Value Problems
a SpringerOpen Journal

RESEARCH Open Access

Bifurcations, chaotic behavior, sensitivity analysis, and various soliton solutions for the extended nonlinear Schrödinger equation

Mati ur Rahman[1,2], Mei Sun[1*], Salah Boulaaras[3*] and Dumitru Baleanu[2]

*Correspondence:
sunm@ujs.edu.cn;
s.boularas@qu.edu.sa
[1]School of Mathematical Sciences, Jiangsu University, Zhenjiang, 212013, Jiangsu, P.R. China
[3]Department of Mathematics, College of Sciences and Arts in ArRass, Qassim University, Buraydah, 51452, Saudi Arabia
Full list of author information is available at the end of the article

Abstract

In this manuscript, our primary objective is to delve into the intricacies of an extended nonlinear Schrödinger equation. To achieve this, we commence by deriving a dynamical system tightly linked to the equation through the Galilean transformation. We then employ principles from planar dynamical systems theory to explore the bifurcation phenomena exhibited within this derived system. To investigate the potential presence of chaotic behaviors, we introduce a perturbed term into the dynamical system and systematically analyze the extended nonlinear Schrödinger equation. This investigation is further enriched by the presentation of comprehensive two- and 3D phase portraits. Moreover, we conduct a meticulous sensitivity analysis of the dynamical system using the Runge–Kutta method. Through this analytical process, we confirm that minor fluctuations in initial conditions have only minimal effects on solution stability. Additionally, we utilize the complete discrimination system of the polynomial method to systematically construct single traveling wave solutions for the governing model.

Keywords: Schrödinger equation; Galilean transformation; Traveling wave solutions; Nonlinear equations

1 Introduction

Nonlinear physical phenomena are mathematically captured through a set of equations referred to as nonlinear differential equations. Notably, among these equations, nonlinear partial differential equations (PDEs) emerge as crucial tools for investigating and interpreting nonlinear behaviors. These nonlinear PDEs play a pivotal role in describing a diverse array of physical problems spanning various fields including optics, biology, chemistry, plasma physics, engineering, meteorology, fluid dynamics, oceanography, and aerospace industries [1–3]. Central to the exploration of these phenomena is the quest to find solutions for these intricate mathematical models. Over time, numerous effective approaches have been developed to derive exact solutions for nonlinear PDEs. These methods encompass a range of techniques such as the tanh-coth function method [4], the exponential rational function method [5], the Hirota bilinear method [6], the modi-

Springer

fied exp-function method [7], the generalized Kudryashov method [8], neural networks [9, 10], and others [11, 12].

Amidst the extensive collection of scholarly works, a wide range of soliton solutions has been extensively chronicled. These solutions encompass diverse categories, notably bright solitons, dark solitons, and kink solitons. An exploration led by Chen et al. [13] revealed kink solitons in the context of a 3D Boiti–Leon–Manna–Pempinelli equation, employing the three-wave method. In a separate endeavor, Ding et al. [14] employed the Kadomtsev–Petviashvili hierarchy reduction technique to expose dark solitons within the framework of the Davey–Stewartson II equation. A noteworthy instance involves the work of Tariq et al. [15], in which the authors ingeniously utilized an F-expansion method to derive bright solitons for the (2+1)-dimensional chiral equation. The extended nonlinear and the coupled extended nonlinear Schrödinger equations are studied in [16]. Solitary and traveling wave solutions of 2D generalized Schrödinger equations are studied in [17]. Further, bifurcation, stationary optical solitons, and other exact solutions for the generalized nonlinear Schrödinger equation (NLSE) are presented in [18].

In present-day research, scholars grapple with a diverse spectrum of nonlinear PDEs and their corresponding dynamic systems. The accessibility of sophisticated symbolic packages has significantly enhanced researchers' understanding of dynamic systems, enabling comprehensive analysis [19, 20]. Approaches to investigating dynamic systems encompass multifaceted perspectives, spanning bifurcation analysis, examination of chaotic behaviors, and sensitivity analysis [21–25]. Notably, recent scholarly attention has increasingly focused on these realms of dynamic systems. This burgeoning interest is prominently evident in inquiries concerning prominent PDEs. Illustrative examples encompass the Hirota–Maccari system [26], the coupled Kundu–Mukherjee–Naskar equation [27], investigations into the generalized Schrödinger equation [28], explorations of the modified Gardner equation [29], and the study of the generalized q-deformed Sinh–Gordon equation [30].

The propagation of femtosecond pulses within a single-mode optical fiber is mathematically characterized by the extended NLSE. This equation, as introduced by Kodama and Hasegawa in [31] and further developed by Gordon in [32], as well as Mitschke and Mollenauer in [33], serves as a fundamental framework for describing the intricate dynamics of ultra-short optical pulses as they traverse through optical fibers. This paper is dedicated to a comprehensive exploration of the extended NLSE:

$$\iota(\mathcal{U}_x + \Re_1\mathcal{U}_t) - \frac{\Re_2}{2}\mathcal{U}_{tt} + \rho|\mathcal{U}|^2\mathcal{U} + \iota\lambda_1\left(|\mathcal{U}|^2\mathcal{U}\right)_t + \iota\lambda_2\left(|\mathcal{U}|^2\right)_t\mathcal{U} - \iota\frac{\Re_3}{6}\mathcal{U}_{ttt} = 0, \tag{1}$$

where $\mathcal{U}$ is the slowly varying envelope of the electric field, dependent on variables x and t. The parameter $\Re_1$ represents the inverse of the group velocity, while $\Re_2$ characterizes the second-order dispersion (SOD). Additionally, $\Re_3$ pertains to the third-order dispersion (TOD) parameter, λ_1 corresponds to the coefficient of the derivative cubic term, λ_2 relates to the self-frequency shift of solitons, and ρ signifies the effective nonlinear coefficient.

The extended NLSE presents a versatile and powerful tool for understanding and predicting a wide array of complex wave phenomena. Its adaptability allows for the exploration of nonlinear effects in diverse systems, including optical pulse propagation, with precision and depth. This equation's ability to provide both analytical and numerical solutions facilitates in-depth insights into nonlinear wave dynamics, offering researchers a comprehensive framework to study simple solitons, intricate breathers, and extreme

events like rogue waves. In practical applications, it plays a pivotal role in designing and optimizing optical communication systems, enabling the development of high-capacity data transmission technologies and signal processing techniques. Overall, the extended NLSE stands as a cornerstone in the study of nonlinear wave behavior, enhancing our understanding and control of complex wave patterns.

Numerous prior investigations have delved into the extended NLSE. For instance, there have been studies on exact solutions considering third-order and nonlinear dispersion effects, as demonstrated in Ozisik et al. [34] and Borich et al. [35], respectively. Researchers have also explored breather and rogue wave solutions, encompassing higher-order odd and even terms, as outlined in Su et al. [36]. Additionally, investigations into higher-order smooth positon and breather positon solutions have been conducted (Monisha et al. [37]). The extended NLSE has been examined in the context of quadratic and cubic nonlinearities (Sedletsky et al. [38]) and in the realm of two-breather solutions for the class I infinitely extended NLSE (Crabb and Akhmediev [39]). Soliton solutions, rational soliton solutions, and rogue wave solutions have been the focus of studies, exemplified by Huang et al. [40]. Furthermore, breather and rogue wave solutions have been explored through the generalized Darboux transformation, as elucidated by Lou et al. [41].

Several chaotic systems composed of 2D ODEs have been introduced from time to time, contributing to the rich field of chaos theory. One notable example of a well-known 2D chaotic system is the Hénon map [42], defined by iteratively updating two variables based on a set of nonlinear equations. Further, the 2D sine-logistic-tent-coupling map has been introduced [43]. Similarly, a new 2D hyperchaotic system is presented in [44]. Researchers often study these 2D chaotic systems to understand the fundamental principles of chaotic dynamics, bifurcation phenomena, and sensitivity to initial conditions. The exploration of such systems not only advances theoretical aspects of chaos theory but also finds applications in secure communication, random number generation, and diverse fields where pseudorandom and unpredictable behavior are desirable.

The primary objective of this manuscript is to deeply explore the dynamics encapsulated by the given equation. The journey commences by employing the Galilean transformation as a foundational step, leading to the derivation of a corresponding dynamical system associated with Eq. (1). The Galilean transformation serves as a valuable tool when it comes to converting PDEs into systems of ordinary differential equations (ODEs), especially in the context of classical mechanics. This transformation is essential for handling problems involving relative motion between different inertial reference frames. In the process of converting PDEs to ODEs, the Galilean transformation allows for the seamless transition from a frame of reference moving at a constant velocity to a stationary frame. By appropriately accounting for this relative motion, the terms involving spatial derivatives in the original PDEs can be reformulated into terms involving only time derivatives. This transformation simplifies the mathematical analysis and facilitates the solution of the resulting system of ODEs. Consequently, the Galilean transformation provides a powerful mathematical framework for studying physical phenomena in classical mechanics, allowing researchers to gain deeper insights into the dynamics of systems through the more manageable lens of ODEs.

Furthermore, utilizing the well-established theory of planar dynamical systems, a thorough bifurcation analysis is meticulously conducted, shedding light on the intricate behaviors exhibited by the system. This investigation goes beyond bifurcations [45–47], delving

into the realm of chaotic phenomena within the governed model. To accomplish this, a dynamical system is studied, augmented with an external term. The exploration of chaotic behaviors involves constructing and examining a series of 2D and 3D phase portraits, providing a comprehensive understanding of the intricate dynamics at play. In the extant literature, a number of notable publications have been carefully studied in the broad field of soliton solutions and bifurcation. These studies explore the complex dynamics of nonlinear systems, providing insight into the intriguing behavior of solitons and the bifurcation processes that control it [48, 49].

Moreover, this research employs the Runge–Kutta method to perform sensitivity analysis of the dynamical system. This investigation ensures the robustness and stability of the solutions against minor perturbations in initial conditions. By subjecting the system to slight variations and analyzing their impact on stability, this study contributes to validating the reliability and consistency of the derived solutions. A comprehensive explanation of bifurcation analysis for the unperturbed dynamical system is presented, complemented by detailed phase portraits. The exploration of chaos in the perturbed dynamical system is carried out, utilizing various techniques to identify chaotic patterns in both time series and phase portraits. Additionally, the authors employ the complete discrimination system of the polynomial method to construct single traveling wave solutions of the governing model. Notably, we emphasize the novelty of this study, asserting that such an investigation has not been previously undertaken within the context of the discussed system.

The organization of this paper is as follows. In Sect. 2, the focus shifts towards deriving the dynamical system that corresponds to Eq. (1). In Sect. 3, a thorough exploration encompassing bifurcation analysis, chaotic phenomena, and sensitivity analysis concerning the governing equation is presented. Moving on to Sect. 4, our attention is directed to the investigation of traveling wave solutions. Lastly, Sect. 5 assumes the role of a reflective synopsis, succinctly summarizing the achievements and discoveries presented in this study.

2 Dynamical system of the governing equation

Let us contemplate the ensuing complex transformation

$$\mathcal{U}(x,t) = e^{\iota\Omega}\mathcal{G}(\delta), \tag{2}$$

where $\delta = t - \xi x + \delta_0$ and $\Omega = \nu x - \kappa t + \Omega_0$. Substituting Eq. (2) into Eq. (1), we derive a nonlinear ODE. This equation, upon separation into its imaginary and real components, yields the following:

$$-\Re_3\frac{d^3\mathcal{G}(\delta)}{d\delta^3} + \left(6(3\lambda_1+2\lambda_2)\left(\mathcal{G}(\delta)\right)^2 + 3\left(\kappa^2\Re_3 + 2\kappa\Re_2 - 2\xi + 2\Re_1\right)\right)\frac{d\mathcal{G}(\delta)}{d\delta} = 0, \tag{3}$$

$$6(\kappa\lambda_1+\rho)\left(\mathcal{G}(\delta)\right)^3 + \left(\kappa^3\Re_3 + 3\kappa^2\Re_2 + 6(\kappa\Re_1 - \nu)\right)\mathcal{G}(\delta) + (-3\kappa\Re_3 - 3\Re_2)\frac{d^2\mathcal{G}(\delta)}{d\delta^2} = 0. \tag{4}$$

After integrating Eq. (3) with respect to δ once and assuming the integration constant to be zero, we arrive at the following:

$$2(3\lambda_1+2\lambda_2)\left(\mathcal{G}(\delta)\right)^3 + 3\left(\kappa^2\Re_3 + 2(\kappa\Re_2 - \xi + \Re_1)\right)\mathcal{G} - \Re_3\frac{d^2\mathcal{G}(\delta)}{d\delta^2} = 0. \tag{5}$$

From Eq. (4) and Eq. (5), we have

$$\frac{3(\kappa\lambda_1+\rho)}{3\lambda_1+2\lambda_2}=\frac{\kappa^3\Re_3+3\kappa^2\Re_2+\kappa\Re_1-6\nu}{3(\kappa^2\Re_3+2(\kappa\Re_2-\xi+\Re_1))}=\frac{3(\kappa\Re_3+\Re_2)}{\Re_3}. \tag{6}$$

One can reach the following constraint from the above proposition:

$$\begin{aligned}\xi&=\frac{4\kappa^3\Re_3^2+12\kappa^2\Re_2\Re_3+6\kappa\Re_1\Re_3+9\kappa\Re_2^2+3\nu\Re_3+9\Re_1\Re_2}{9(\kappa\Re_3+\Re_2)},\\ \rho&=\frac{2\Re_2(\kappa\lambda_1+\kappa\lambda_2)+\Re_2(3\lambda_1+2\lambda_2)}{\Re_3}.\end{aligned} \tag{7}$$

Upon implementing the Galilean transformation to Eq. (4), we obtain the dynamical system as follows:

$$\begin{cases}\frac{d\mathcal{G}(\delta)}{d\delta}=\mathcal{P},\\ \frac{d\mathcal{P}(\delta)}{d\delta}=\mathcal{W}_1\mathcal{G}^3(\delta)+\mathcal{W}_2\mathcal{G}(\delta),\end{cases} \tag{8}$$

where

$$\begin{aligned}\mathcal{W}_1&=\frac{6(\kappa\lambda_1+\rho)}{3\kappa\Re_3+3\Re_2},\\ \mathcal{W}_2&=\frac{(\kappa^3\Re_3+3\kappa^2\Re_2+6(\kappa\Re_1-\nu))}{3\kappa\Re_3+3\Re_2}.\end{aligned} \tag{9}$$

3 The exploration of bifurcation analysis, chaotic behavior, and sensitivity analysis pertaining to the governing equation

In this section, a comprehensive examination of bifurcation analysis, chaotic behavior, and sensitivity analysis is provided for the governing equation.

3.1 Bifurcation analysis

In this subsection, we present the bifurcation analysis, including phase portraits, of the dynamical system given by Eq. (8). Firstly, we express the Hamiltonian function for Eq. (8) as follows:

$$\mathcal{H}(\mathcal{G},\mathcal{P})=\frac{\mathcal{P}^2}{2}-\frac{\mathcal{W}_1\mathcal{G}^4}{4}-\frac{\mathcal{W}_2\mathcal{G}^2}{2}=\mathsf{h},$$

where h is the Hamiltonian constant. We solve the system

$$\begin{cases}\mathcal{P}=0,\\ \mathcal{W}_1\mathcal{G}^3+\mathcal{W}_2\mathcal{G}=0\end{cases}$$

to derive the equilibrium points (Eqps) of (8). The derived Eqps are

$$\mathcal{E}_1=(0,0),\qquad \mathcal{E}_2=\left(-\iota\sqrt{\frac{\mathcal{F}_2}{\mathcal{F}_1}},0\right),\qquad \mathcal{E}_2=\left(\iota\sqrt{\frac{\mathcal{F}_2}{\mathcal{F}_1}},0\right).$$

The Jacobian matrix determinant of system (8) is

$$\mathcal{D}(\mathcal{G},\mathcal{P}) = \begin{vmatrix} 0 & 1 \\ 3\mathcal{W}_1\mathcal{G}^2 + \mathcal{W}_2 & 0 \end{vmatrix} = -3\mathcal{W}_1\mathcal{G}^2 - \mathcal{W}_2.$$

We know that:

1. $(\mathcal{G},\mathcal{P})$ is a saddle point if $\mathcal{D}(\mathcal{G},\mathcal{P}) < 0$;
2. $(\mathcal{G},\mathcal{P})$ is a center point if $\mathcal{D}(\mathcal{G},\mathcal{P}) > 0$;
3. $(\mathcal{G},\mathcal{P})$ is a cuspid point if $\mathcal{D}(\mathcal{G},\mathcal{P}) = 0$;

The outcomes that may be attained by altering the pertinent parameter are listed below.

Case 1: $\mathcal{W}_1 > 0$ and $\mathcal{W}_2 > 0$

By selecting specific values for the parameters $\mathfrak{K}_1 = 1$, $\mathfrak{K}_2 = 2$, $\mathfrak{K}_3 = 1$, $\nu = 0.4$, $\kappa = 1$, $\rho = 2$, and $\lambda_1 = 1$, we discover that the only real Eqp is $(0,0)$, as depicted in Fig. 1(a). Evidently, $(0,0)$ corresponds to a saddle point.

Case 2: $\mathcal{W}_1 < 0$ and $\mathcal{W}_2 > 0$

After selecting the parameters $\mathfrak{K}_1 = 1$, $\mathfrak{K}_2 = 2$, $\mathfrak{K}_3 = 1$, $\nu = 0.4$, $\kappa = 1$, $\rho = -2$, and $\lambda_1 = 1$, we observe that there are three Eqps, $(0,0)$, $(-1.3292,0)$, and $(1.3292,0)$, in which $(0,0)$ acts as a saddle point, as illustrated in Fig. 1(b). Furthermore, $(-1.3292,0)$ and $(1.3292,0)$ act as center points.

Case 3: $\mathcal{W}_1 < 0$ and $\mathcal{W}_2 < 0$

By selecting the parameters $\mathfrak{K}_1 = -0.1$, $\mathfrak{K}_2 = 2$, $\mathfrak{K}_3 = 1$, $\nu = 0.4$, $\kappa = 1$, $\rho = -2$, and $\lambda_1 = 1$, we identify that the only noncomplex real Eqp is $(0,0)$, as depicted in Fig. 1(c). Evidently, $(0,0)$ corresponds to a center point.

Case 4: $\mathcal{W}_1 > 0$ and $\mathcal{W}_2 < 0$

By selecting the parameters $\mathfrak{K}_1 = 1$, $\mathfrak{K}_2 = 2$, $\mathfrak{K}_3 = 1$, $\nu = 5.4$, $\kappa = 1$, $\rho = 2$, and $\lambda_1 = 1$, we identify that there are three Eqps, which are $(0,0)$, $(-1.0382,0)$, and $(1.0382,0)$, as depicted in Fig. 1(d). Evidently, $(0,0)$ corresponds to a center point, while $(-1.0382,0)$ and $(1.0382,0)$ represent saddle points.

3.2 Chaotic behavior of the governing equation

In this subsection, we explore the existence of chaotic behavior in the resulting system (8) by introducing a perturbed term. We analyze 2D and 3D phase portraits for this system. The following dynamical system is considered:

$$\begin{cases} \frac{d\mathcal{G}(\mathrm{t})}{d\mathrm{t}} = \mathcal{P}, \\ \frac{d\mathcal{P}(\mathrm{t})}{d\mathrm{t}} = \mathcal{W}_1\mathcal{G}^3(\mathrm{t}) + \mathcal{W}_2\mathcal{G}(\mathrm{t}) + \omega\cos^2(\mu\mathrm{t}), \quad \omega \neq 0, \mu \neq 0. \end{cases} \tag{10}$$

In the following figures, we examine the influence of the perturbed term $\omega\cos^2(\mu t)$ on the dynamical system given by Eq. (10). Here, ω and μ represent the amplitude and frequency of the system, respectively.

We present both 2D and 3D phase portraits of the system for the parameters $\mathfrak{K}_1 = 1$, $\mathfrak{K}_2 = 2$, $\mathfrak{K}_3 = 1$, $\nu = 0.4$, $\kappa = 1$, $\rho = 2$, and $\lambda_1 = 1$, while the parameters ω and μ are varied: in Fig. 2(a), $\omega = 1$, $\mu = 1$; in Fig. 2(b), $\omega = 0.8$, $\mu = 1$; in Fig. 3(a), $\omega = 1$, $\mu = 0.9$; and in Fig. 3(b), $\omega = 1$, $\mu = 0.1$. On analyzing the phase diagrams, we see complex and mesmerizing behaviors. In Fig. 2(a) we see the four scroll dynamics, while in Fig. 2(b) complex dynamics are observed. Furthermore, in Fig. 3(a), periodic dynamics can be observed, while

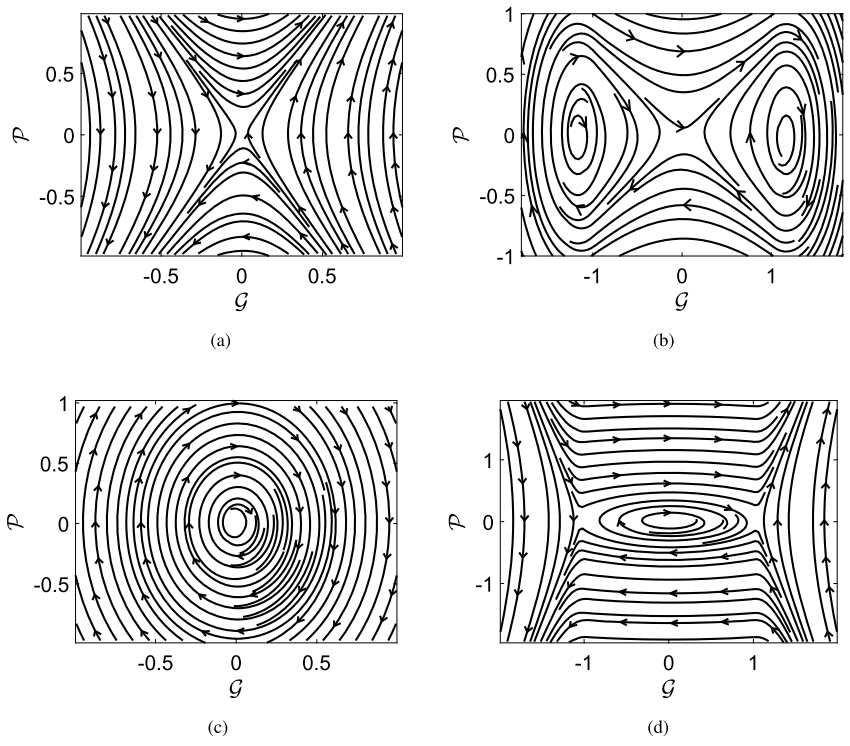

Figure 1 Phase portraits of the proposed system's bifurcations with various conditions for $\mathcal{W}_1$ and $\mathcal{W}_2$ based on different parameter values

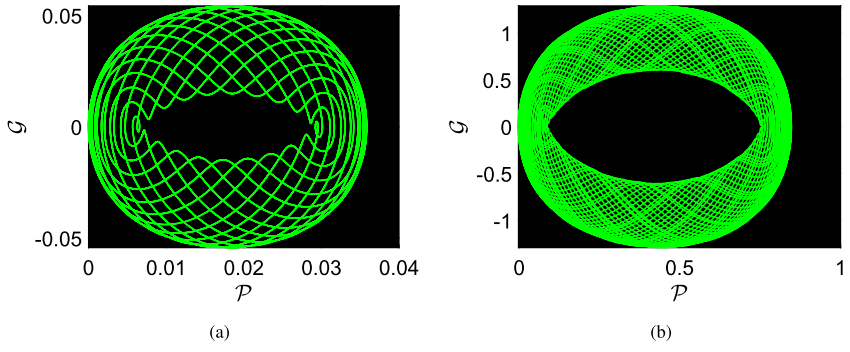

Figure 2 Chaotic visualizations of the proposed equation with parameters assumed as $\mathfrak{K}_1 = 1$, $\mathfrak{K}_2 = 2$, $\mathfrak{K}_3 = 1$, $\nu = 0.4$, $\kappa = 1$, $\rho = 2$, and $\lambda_1 = 1$

Fig. 3(b) shows strange periodic dynamics. These discoveries illuminate the system's dynamics' susceptibility to fluctuations in the parameter μ, offering profound insights into how the perturbed term $\omega \cos^2(\mu t)$ influences the system's global behavior. This newfound understanding of the system's sensitivity to parameter variations enhances our grasp of the intricate relationship between μ, the perturbation term, and the overall system dynamics. Such insights contribute significantly to the broader comprehension of how even subtle changes in parameters can steer the trajectory of the system, ultimately paving the way for more informed and accurate predictions of its behavior under varying conditions.

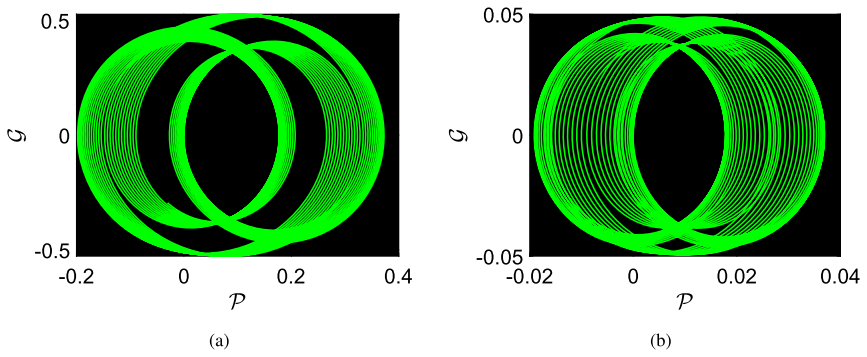

Figure 3 Chaotic visualizations of the proposed equation with parameters assumed as $\mathfrak{K}_1 = 1$, $\mathfrak{K}_2 = 2$, $\mathfrak{K}_3 = 1$, $\nu = 0.4$, $\kappa = 1$, $\rho = 2$, and $\lambda_1 = 1$

3.3 Sensitivity analysis of the governing equation

Here, we employ the well-known and efficient Runge–Kutta method to analyze the sensitivity of the dynamical system represented by Eq. (8). To achieve this, we solve the following dynamical system using the Runge–Kutta method:

$$\begin{cases} \frac{d\mathcal{G}(\mathrm{t})}{d\mathrm{t}} = \mathcal{P}, \\ \frac{d\mathcal{P}(\mathrm{t})}{d\mathrm{t}} = \mathcal{W}_1\mathcal{G}^3(\mathrm{t}) + \mathcal{W}_2\mathcal{G}(\mathrm{t}). \end{cases} \tag{11}$$

The values of the parameters are set as follows: $\mathfrak{K}_1 = 1$, $\mathfrak{K}_2 = 2$, $\mathfrak{K}_3 = 1$, $\nu = 0.4$, $\kappa = 1$, $\rho = 2$, and $\lambda_1 = 1$. The initial conditions for the system are given by:

(a) $\mathcal{G}(0) = 0.1$ and $\mathcal{P} = 0$; (b) $\mathcal{G}(0) = 0$ and $\mathcal{P} = 0.1$;

(c) $\mathcal{G}(0) = 0.2$ and $\mathcal{P} = 0$; (d) $\mathcal{G}(0) = 0$ and $\mathcal{P} = 0.2$.

The results obtained from this effective scheme are depicted in Fig. 4. The blue curves show the dynamics of class $\mathcal{G}$, while the red ones depict $\mathcal{P}$'s dynamics. Looking at the figures, it is clear that small changes in the initial conditions lead to considerable changes in the dynamics of the system.

4 Traveling wave solution of the governing equation

This section of the manuscript is dedicated to a comprehensive analysis of the novel traveling wave solutions arising from the governing equation under consideration. The exploration of these solutions is pivotal in unraveling the intricate dynamics embedded within the system. This analytical approach not only contributes to the theoretical framework of the study but also lays the foundation for potential applications and implications in diverse scientific and engineering domains. The elucidation of these novel traveling wave solutions is expected to broaden our insights into the complex dynamics of the system, further substantiating the significance and innovation encapsulated within the research endeavor. By delving into the characteristics and properties of these traveling wave solutions, we aim to provide a deeper understanding of the underlying mechanisms governing the system's behavior. To achieve this objective, Eq. (4) can be reformulated as follows:

$$\mathcal{W}_1\mathcal{G}^3(\delta) + \mathcal{W}_2\mathcal{G}(\delta) = \mathcal{G}''(\delta). \tag{12}$$

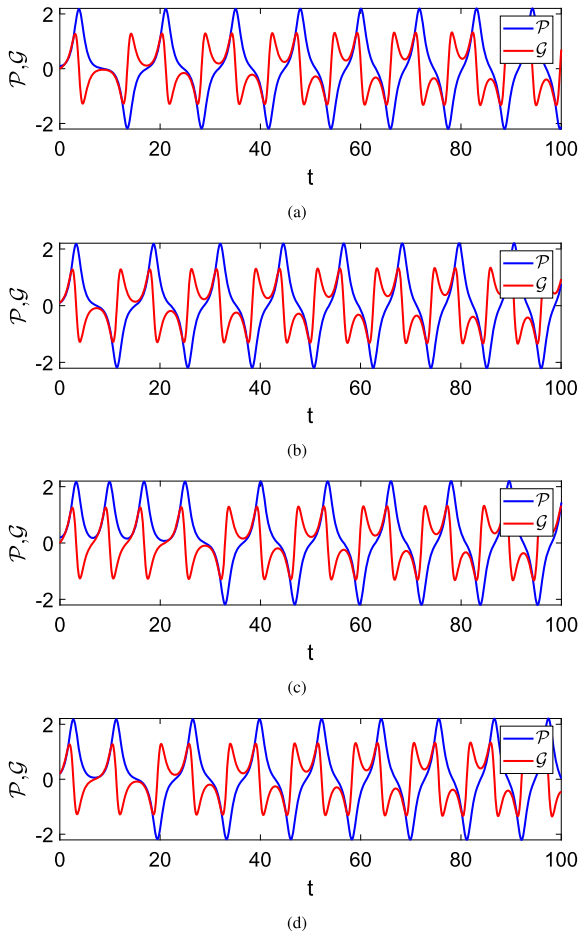

Figure 4 Numerical demonstrations of the state variables vs. t with parameters considered as $\mathfrak{K}_1 = 1$, $\mathfrak{K}_2 = 2$, $\mathfrak{K}_3 = 1$, $\nu = 0.4$, $\kappa = 1$, $\rho = 2$, and $\lambda_1 = 1$ with different initial values

Multiplying $\mathcal{G}'$ on both sides of Eq. (12) and integrating, we obtain

$$\left(\mathcal{G}'\right)^2 = \frac{\mathcal{W}_1}{2} + \mathcal{W}_2\mathcal{G}^2 + 2\mathcal{W}_0, \tag{13}$$

where $\mathcal{W}_0$ is the constant. We take the following transformation:

$$\mathcal{G} = \pm\sqrt{(2\mathcal{W}_1)^{-\frac{1}{3}}\Psi}, \mathsf{p} = 4\mathcal{W}_2(2\mathcal{W}_1)^{-\frac{2}{3}}, \mathsf{q} = 8\mathcal{W}_0(2\mathcal{W}_1)^{-\frac{1}{3}}, \delta_1 = (2\mathcal{W}_1)^{\frac{1}{3}}\delta. \tag{14}$$

Then from Eq. (12), we obtain

$$(\Psi_{\delta_1})^2 = \Psi\left(\Psi^2 + \mathsf{p}\Psi + \mathsf{q}\right). \tag{15}$$

Now, we can obtain the integral of Eq. (15) as

$$\pm(\delta_1 - \delta_0) = \int \frac{d\Psi}{\sqrt{\Psi(\Psi^2 + \mathsf{p}\Psi + \mathsf{q})}}. \tag{16}$$

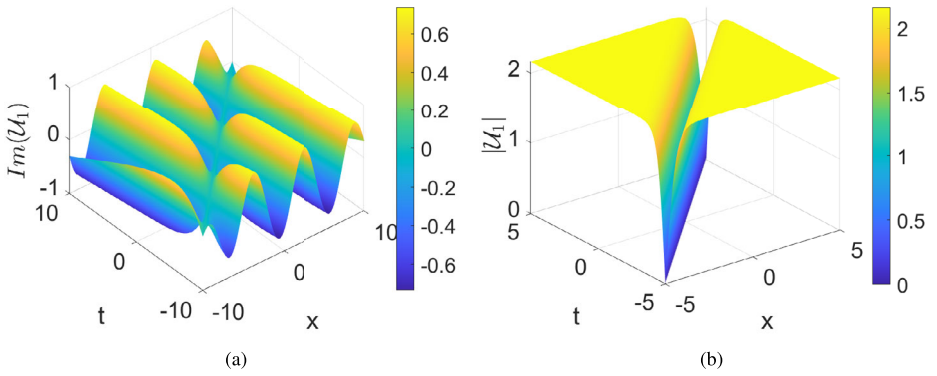

Figure 5 Numerical visualizations of exact solution $\mathcal{U}_1$ with parameters $\mathfrak{K}_1 = -1$, $\mathfrak{K}_2 = 3$, $\mathfrak{K}_3 = 1$, $\nu = 0.4$, $\kappa = 1$, $\rho = 2$, $\lambda_1 = 1$, $\xi = 2$, $\delta_0 = 1$, and $\Omega_0 = 0$

In this context, we establish $\mathcal{F}(\Psi)$ as $\Psi^2 + \mathsf{p}\Psi + \mathsf{q}$, and we introduce $\mho$ as $\mathsf{p}^2 - 4\mathsf{q}$. Based on the roots of the equation $\mathcal{F}(\Psi) = 0$, the solution to Eq. (16) manifests in four distinct scenarios.

Case: 1 $\mho = 0$ and $\Psi > 0$.

When $\mathsf{p} < 0$ and $\mathcal{W}_2 < 0$, the solution of Eq. (1) is given by

$$\mathcal{U}_1(x,t) = \pm\sqrt{-\frac{\mathcal{W}_2}{\mathcal{W}_1}\tanh^2\left(\frac{(-2\mathcal{W}_2)^{\frac{1}{2}}}{2}(t-\xi x+\delta_0)\right)}e^{\iota(\nu x-\kappa t+\Omega_0)}, \tag{17}$$

The exact solution, denoted as $\mathcal{U}_1$, is subjected to numerical simulation in Fig. 5 using carefully chosen parameters. The simulation results are visually represented, with Fig. 5(a) showcasing the imaginary component of the solution and Fig. 5(b) portraying the absolute characteristics of $\mathcal{U}_1$. These visualizations provide valuable insights into the physical interpretation of the solution. In Fig. 5(a), the observed behavior of the imaginary component reveals a notable feature known as dark solitons. Dark solitons are intriguing nonlinear wave phenomena that describe localized, low-intensity regions within a broader wave profile. The dark soliton behavior, as seen in the simulation, signifies a stable, solitary wave with a phase difference from its surroundings. This physical demonstration not only verifies the theoretical solution but also showcases the presence of dark solitons in the system, which holds significance in various fields, including optics, fluid dynamics, and plasma physics. The absolute behavior of $\mathcal{U}_1$, as shown in Fig. 5(b), further confirms the characteristics of these dark solitons and underscores their relevance in understanding nonlinear wave dynamics and localized wave structures. We have

$$\mathcal{U}_2(x,t) = \pm\sqrt{-\frac{\mathcal{W}_2}{\mathcal{W}_1}\coth^2\left(\frac{(-2\mathcal{W}_2)^{\frac{1}{2}}}{2}(t-\xi x+\delta_0)\right)}e^{\iota(\nu x-\kappa t+\Omega_0)}, \tag{18}$$

The exact solution $\mathcal{U}_2$ is physically illustrated through numerical simulations in Fig. 6, using well-suited parameters. In Fig. 6(a), the observed behavior corresponds to the imaginary component of the solution, while Fig. 6(b) presents the absolute characteristics of $\mathcal{U}_2$. The results clearly manifest a distinctive phenomenon – the singular soliton solution. Singular solitons are exceptional in that they exhibit highly localized, self-contained wave

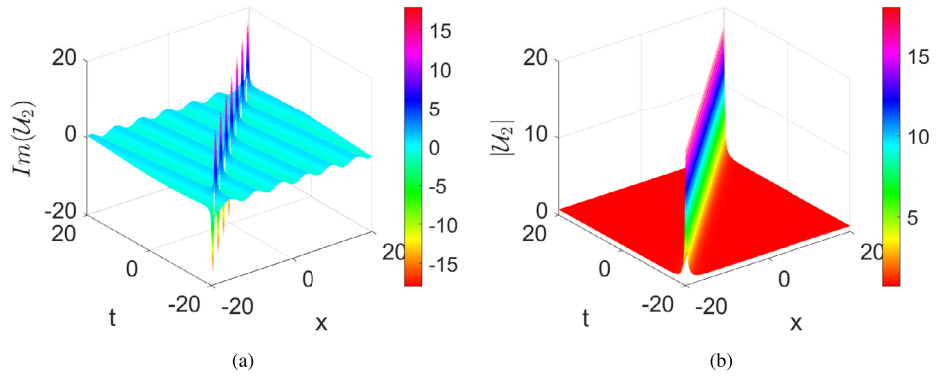

Figure 6 Numerical visualizations of exact solution $\mathcal{U}_2$ with parameters $\mathfrak{K}_1 = -1$, $\mathfrak{K}_2 = 3$, $\mathfrak{K}_3 = 1$, $\nu = 0.4$, $\kappa = 1$, $\rho = 2$, $\lambda_1 = 1$, $\xi = 2$, $\delta_0 = 1$, and $\Omega_0 = 0$

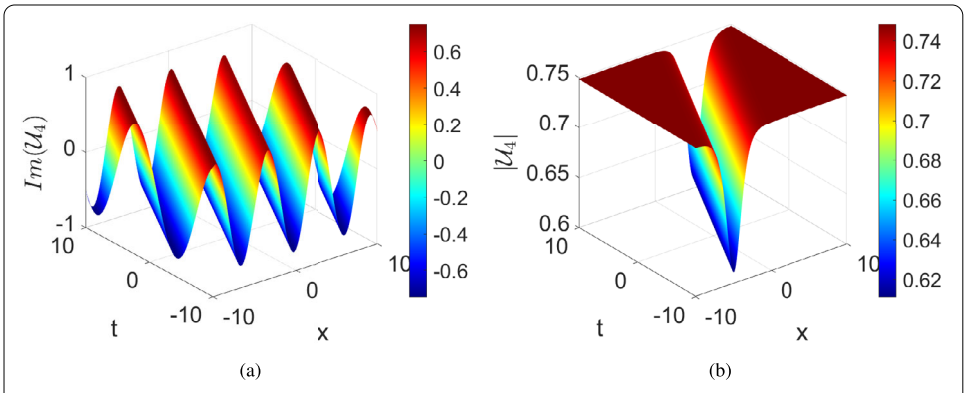

Figure 7 Numerical visualizations of exact solution $\mathcal{U}_4$ with parameters $\mathfrak{K}_1 = 0.1$, $\mathfrak{K}_2 = 3$, $\mathfrak{K}_3 = 1$, $\nu = 1.4$, $\kappa = 1.2$, $\rho = 1.2$, $\lambda_1 = 1$, $\xi = 2$, $\delta_0 = 1$, and $\Omega_0 = 0$

structures with remarkable features, including infinite intensity and an abrupt phase jump. The existence of a singular soliton solution, as evidenced in this demonstration, not only validates the theoretical prediction but also underscores the presence of these extraordinary structures within the system. The study of singular solitons holds profound significance in various branches of physics, as they represent nondispersive and localized wave phenomena, offering insights with applications in optics, plasma physics, and fluid dynamics.

When $\mathsf{p} > 0$ and $\mathcal{W}_2 > 0$, the solution of Eq. (1) is given by

$$\mathcal{U}_3(x,t) = \sqrt{\frac{\mathcal{W}_2}{\mathcal{W}_1}\tan^2\left(\frac{(2\mathcal{W}_2)^{\frac{1}{2}}}{2}(t-\xi x+\delta_0)\right)}e^{\iota(\nu x-\kappa t+\Omega_0)}, \tag{19}$$

When $\mathsf{p} = 0$ and $\mathcal{W}_2 > 0$, the solution of Eq. (1) is given by

$$\mathcal{U}_4(x,t) = \pm\sqrt{\frac{2}{\mathcal{W}_1(t-\xi x+\delta_0)^2}}e^{\iota(\nu x-\kappa t+\Omega_0)}, \tag{20}$$

The concrete representation of the exact solution, denoted as $\mathcal{U}_4$, is achieved through nu-

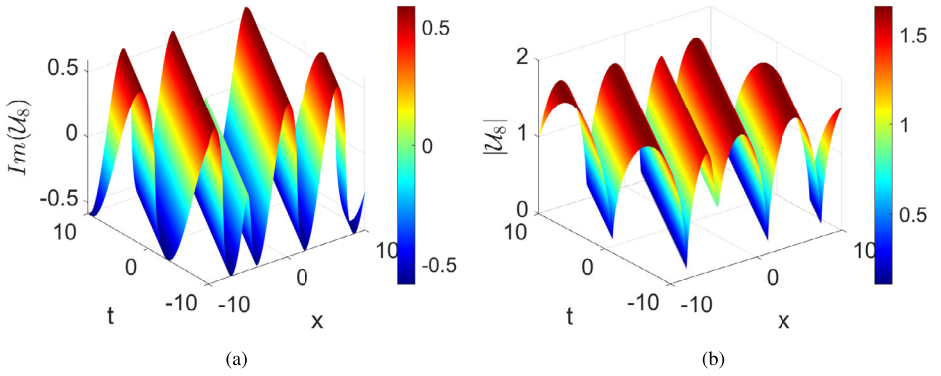

Figure 8 Numerical visualizations of exact solution $\mathcal{U}_8$ with parameters $\mathfrak{K}_1 = 0.1$, $\mathfrak{K}_2 = 3$, $\mathfrak{K}_3 = 1$, $\nu = 1.4$, $\kappa = 1.2$, $\rho = 1.2$, $\lambda_1 = 1$, $s_1 = 0$, $s_2 = 1$, $s_3 = 2$, $\xi = 2$, $\delta_0 = 1$, and $\Omega_0 = 0$

merical simulations in Fig. 7, utilizing well-tailored parameters. Figure 7(a) effectively portrays the behavior of the solution's imaginary component, while Fig. 7(b) vividly displays the absolute characteristics of $\mathcal{U}_4$. In this visualization, we witness the existence of periodic waves. These periodic waves exhibit recurrent, self-replicating patterns that preserve their shape and periodic nature as they travel through the system. However, the overall behavior, as depicted in Fig. 7(b), unveils an additional intriguing aspect – the existence of dark wave solutions.

Case: 2 $\mho > 0$ and $\mathsf{q} = 0$

When $\Psi > -\mathsf{p}$ and $\mathsf{p} < 0$, the solution of Eq. (1) is given by

$$\mathcal{U}_5(x,t) = \pm\sqrt{\frac{\mathcal{W}_2}{\mathcal{W}_1}\tanh^2\left(\frac{(2\mathcal{W}_2)^{\frac{1}{2}}}{2}(t-\xi x+\delta_0)\right) - \frac{2\mathcal{W}_2}{\mathcal{W}_1}}e^{\iota(\nu x-\kappa t+\Omega_0)}, \tag{21}$$

$$\mathcal{U}_6(x,t) = \sqrt{\frac{\mathcal{W}_2}{\mathcal{W}_1}\coth^2\left(\frac{(2\mathcal{W}_2)^{\frac{1}{2}}}{2}(t-\xi x+\delta_0)\right) - \frac{2\mathcal{W}_2}{\mathcal{W}_1}}e^{\iota(\nu x-\kappa t+\Omega_0)}. \tag{22}$$

When $\Psi > -\mathsf{p}$ and $\mathsf{p} > 0$, the solution of Eq. (1) is given by

$$\mathcal{U}_7(x,t) = \pm\sqrt{-\frac{\mathcal{W}_2}{\mathcal{W}_1}\tan^2\left(\frac{(-2\mathcal{W}_2)^{\frac{1}{2}}}{2}(t-\xi x+\delta_0)\right) + \frac{2\mathcal{W}_2}{\mathcal{W}_1}}e^{\iota(\nu x-\kappa t+\Omega_0)}. \tag{23}$$

Case: 3 $\mho > 0$ and $\mathsf{p} \neq 0$

Let there exist constants $\mathsf{s}_1, \mathsf{s}_2, \mathsf{s}_3$ satisfying the conditions $\mathsf{s}_1 < \mathsf{s}_2 < \mathsf{s}_3$. Among these constants, one is zero, while the other two serve as the roots of $\mathcal{F}(\Psi) = 0$. In this scenario, the solution to Eq. (1) can be derived as follows:

$$\mathcal{U}_8(x,t) = \pm\sqrt{(2\mathcal{W}_1)^{-\frac{1}{3}}\left[\mathsf{s}_1 + (\mathsf{s}_2-\mathsf{s}_1)sn^2\left(\frac{\sqrt{\mathsf{s}_3-\mathsf{s}_1}}{2}(2\mathcal{W}_1)^{\frac{1}{3}}(t-\xi x+\delta_0), \mathsf{m}\right)\right]} \times e^{\iota(\nu x-\kappa t+\Omega_0)}. \tag{24}$$

The practical manifestation of the exact solution, denoted as $\mathcal{U}_7$, is carried out through numerical simulations in Fig. 8, employing carefully selected parameters. Figure 8(a) provides

a visual representation of the solution's imaginary component, while Fig. 8(b) vividly illustrates the absolute behavior of $\mathcal{U}_7$. In this visualization, the remarkable feature observed is that of aperiodic soliton solutions. Aperiodic solitons, unlike their periodic counterparts, do not exhibit recurrent or regular wave patterns. Instead, they represent complex, nonrepeating structures with a unique and irregular behavior. This physical demonstration not only confirms the theoretical solution but also highlights the presence of aperiodic solitons within the system. The existence of such a soliton type is significant, as it adds a layer of complexity to nonlinear wave dynamics and can find applications in various scientific and technological domains, making this observation particularly noteworthy. We have

$$\mathcal{U}_9(x,t) = \pm\sqrt{(2\mathcal{W}_1)^{-\frac{1}{3}}\left[\frac{-\mathsf{s}_2 sn^2(\frac{\sqrt{\mathsf{s}_3-\mathsf{s}_1}}{2}(2\mathcal{W}_1)^{\frac{1}{3}}(t-\xi x+\delta_0),\mathsf{m})+\mathsf{s}_3}{cn^2(\frac{\sqrt{\mathsf{s}_3-\mathsf{s}_1}}{2}(2\mathcal{W}_1)^{\frac{1}{3}}(t-\xi x+\delta_0),\mathsf{m})}\right]}e^{\iota(\nu x-\kappa t+\Omega_0)}, \quad (25)$$

where $\mathsf{m} = \frac{\mathsf{s}_2-\mathsf{s}_1}{\mathsf{s}_3-\mathsf{s}_1}$.

Case: 4 $\mho < 0$.

When $\Psi > \mathsf{s}_2$, we obtain

$$\mathcal{U}_{10} = \pm\sqrt{2\left(\frac{\mathcal{W}_0}{\mathcal{W}_1}\right)^{\frac{1}{2}}\left[\frac{2}{1+cn(2(\mathcal{W}_0\mathcal{W}_1)^{\frac{1}{4}}(t-\xi x+\delta_0),\mathsf{m})}-1\right]}e^{\iota(\nu x-\kappa t+\Omega_0)}, \quad (26)$$

where $\mathsf{m}^2 = \frac{(2\mathcal{W}_0)^{\frac{1}{2}}-\mathcal{W}_2}{2(2\mathcal{W}_0)^{\frac{1}{2}}}$.

5 Conclusion

This study has effectively accomplished its primary objective of conducting an in-depth exploration into the intricacies of the extended NLSE. Through a systematic derivation of the associated dynamical system via the Galilean transformation, coupled with a meticulous investigation of bifurcation phenomena using planar dynamical system theory, the intricate dynamics of the equation have been unveiled. The introduction of perturbations facilitated a comprehensive exploration of chaotic behaviors, which were vividly depicted through phase portraits. The sensitivity analysis, performed using the Runge–Kutta method, convincingly illustrated the stability of solutions even in the presence of minor fluctuations in initial conditions. Furthermore, the application of the complete discrimination system of the polynomial method enabled the systematic construction of solitary traveling wave solutions for the governing model. Ultimately, this study not only enhances our understanding of the equation itself but also underscores the effectiveness of analytical tools in studying complex dynamical systems. This accomplishment sets the stage for future applications in nonlinear dynamics and mathematical physics, fostering new avenues for exploration and advancement in these fields.

Acknowledgements
The authors would like to thank the handling editor, the editor in chief, and the referees for their comments, which improved the final version of the paper.

Data availability
Not applicable.

Declarations

Ethics approval and consent to participate
This article does not contain any study with human or animal subjects.

Consent for publication
Not applicable.

Competing interests
The authors declare no competing interests.

Author contributions
All the authors contributed to the study. MR, SB contributed to the conceptual design of the study. Numerical analysis and simulation are performed by MS. and MR., SB. and DB. carried out the electronics circuit design and experimental implementation. MS., MS and SB contributed analysis of the results and writing of the manuscript. All authors read and approve the final manuscript.

Author details
[1]School of Mathematical Sciences, Jiangsu University, Zhenjiang, 212013, Jiangsu, P.R. China. [2]Department of Computer Science and Mathematics, Lebanese American University, Beirut, Lebanon. [3]Department of Mathematics, College of Sciences and Arts in ArRass, Qassim University, Buraydah, 51452, Saudi Arabia.

Received: 11 November 2023 Accepted: 7 January 2024 Published online: 19 January 2024

References

1. Ahmad, H., et al.: New approach on conventional solutions to nonlinear partial differential equations describing physical phenomena. Results Phys. **41**, 105936 (2022)
2. Saifullah, S., Alqarni, M.M., Ahmad, S., Baleanu, D., Khan, M.A., Mahmoud, E.E.: Some more bounded and singular pulses of a generalized scale-invariant analogue of the Korteweg–de Vries equation. Results Phys. **52**, 106836 (2023)
3. Ahmad, S., Saifullah, S.: Analysis of the seventh order Caputo fractional KdV equation: applications to Sawada–Kotera–Ito and Lax equation. Commun. Theor. Phys. (2023)
4. Naowarat, S., Saifullah, S., Ahmad, S., De la Sen, M.: Periodic, singular and dark solitons of a generalized geophysical KdV equation by using the Tanh–Coth method. Symmetry **15**(1), 135 (2023)
5. Fadhal, E., et al.: Extraction of exact solutions of higher order Sasa–Satsuma equation in the sense of beta derivative. Symmetry **14**(11), 2390 (2022)
6. Saifullah, S., Ahmad, S., Alyami, M.A., Inc, M.: Analysis of interaction of lump solutions with kink-soliton solutions of the generalized perturbed KdV equation using Hirota-bilinear approach. Phys. Lett. A **454**, 128503 (2022)
7. Attaullah, et al.: Modified exp-function method to find exact solutions of ionic currents along microtubules. Mathematics **10**(6), 851 (2022)
8. Saifullah, S., Fatima, N., Abdelmohsen, S.A.M., Alanazi, M.M., Ahmad, S., Baleanu, D.: Analysis of a conformable generalized geophysical KdV equation with Coriolis effect. Alex. Eng. J. **73**, 651–663 (2023)
9. Li, P.L., Lu, Y.J., Xu, C.J., Ren, J.: Insight into Hopf bifurcation and control methods in fractional order BAM neural networks incorporating symmetric structure and delay. Cogn. Comput. (2023). https://doi.org/10.1007/s12559-023-10155-2
10. Li, P., Gao, R., Xu, C., Shen, J., Ahmad, S., Li, Y.: Exploring the impact of delay on Hopf bifurcation of a type of BAM neural network models concerning three nonidentical delays. Neural Process. Lett. (2022). https://doi.org/10.1007/s11063-022-11118-8
11. Li, B., Zhang, T., Zhang, C.: Investigation of financial bubble mathematical model under fractal-fractional Caputo derivative. Fractals **31**(05), 1–13 (2023)
12. Jiang, X., Li, J., Li, B., Yin, W., Sun, L., Chen, X.: Bifurcation, chaos, and circuit realisation of a new four-dimensional memristor system. Int. J. Nonlinear Sci. Numer. Simul. (2022)
13. Chen, X., Guo, Y., Zhang, T.: Some new kink type solutions for the new (3 + 1)-dimensional Boiti–Leon–Manna–Pempinelli equation. Nonlinear Dyn. **111**(1), 683–695 (2023)
14. Ding, C.-C., et al.: Dynamics of dark and anti-dark solitons for the x-nonlocal Davey–Stewartson II equation. Nonlinear Dyn. **111**(3), 2621–2629 (2023)
15. Tariq, K.U., Wazwaz, A.M., Raza Kazmi, S.M.: On the dynamics of the (2 + 1)-dimensional chiral nonlinear Schrödinger model in physics. Optik **285**, 170943 (2023)
16. Nakkeeran, K.: On the integrability of the extended nonlinear Schrödinger equation and the coupled extended nonlinear Schrödinger equations. J. Phys. A, Math. Gen. **33**(21), 3947 (2000)
17. Burdik, C., Shaikhova, G., Rakhimzhanov, B.: Soliton solutions and traveling wave solutions of the two-dimensional generalized nonlinear Schrödinger equations. Eur. Phys. J. Plus **136**, 1–17 (2021)
18. Han, T., Li, Z., Li, C.: Bifurcation analysis, stationary optical solitons and exact solutions for generalized nonlinear Schrödinger equation with nonlinear chromatic dispersion and quintuple power-law of refractive index in optical fibers. Phys. A, Stat. Mech. Appl. **615**, 128599 (2023)
19. He, Q., ur Rahman, M., Xie, C.: Information overflow between monetary policy transparency and inflation expectations using multivariate stochastic volatility models. Appl. Math. Sci. Eng. **31**(1), 2253968 (2023)
20. Zhu, X., Xia, P., He, Q., Ni, Z., Ni, L.: Coke price prediction approach based on dense GRU and opposition-based learning salp swarm algorithm. Int. J. Bio-Inspir. Comput. **21**(2), 106–121 (2023)
21. Xu, C., Cui, Q., Liu, Z., Pan, Y., Cui, X., Ou, W., ur Rahman, M., Farman, M., Ahmad, S., Zeb, A.: Extended hybrid controller design of bifurcation in a delayed chemostat model. MATCH Commun. Math. Comput. Chem. **90**(3), 609–648 (2023)
22. Xu, C., Liao, M., Li, P., Yao, L., Qin, Q., Shang, Y.: Chaos control for a fractional-order Jerk system via time delay feedback controller and mixed controller. Fractal Fract. **5**(4), 257 (2021)

23. Xu, C., Mu, D., Liu, Z., Pang, Y., Liao, M., Li, P.: Bifurcation dynamics and control mechanism of a fractional-order delayed Brusselator chemical reaction model. MATCH Commun. Math. Comput. Chem. **89**(1), 73–106 (2023)
24. Luo, R., Emadifar, H., ur Rahman, M.: Bifurcations, chaotic dynamics, sensitivity analysis and some novel optical solitons of the perturbed non-linear Schrödinger equation with Kerr law non-linearity. Results Phys. **54**, 107133 (2023)
25. Du, S., Ul Haq, N., ur Rahman, M.: Novel multiple solitons, their bifurcations and high order breathers for the novel extended Vakhnenko–Parkes equation. Results Phys. **54**, 107038 (2023)
26. Han, T., Zhao, L.: Bifurcation, sensitivity analysis and exact traveling wave solutions for the stochastic fractional Hirota–Maccari system. Results Phys. **47**, 106349 (2023)
27. Li, Z., Hu, H.: Chaotic pattern, bifurcation, sensitivity and traveling wave solution of the coupled Kundu–Mukherjee–Naskar equation. Results Phys. **48**, 106441 (2023)
28. Hosseini, K., Hinçal, E., Ilie, M.: Bifurcation analysis, chaotic behaviors, sensitivity analysis, and soliton solutions of a generalized Schrödinger equation. Nonlinear Dyn., 1–8 (2023)
29. Jhangeer, A., et al.: Quasi-periodic, chaotic and travelling wave structures of modified Gardner equation. Chaos Solitons Fractals **143**, 110578 (2021)
30. Kazmi, S.S., et al.: The analysis of bifurcation, quasi-periodic and solitons patterns to the new form of the generalized q-deformed Sinh–Gordon equation. Symmetry **15**(7), 1324 (2023)
31. Kodama, Y., Hasegawa, A.: Nonlinear pulse propagation in a monomode dielectric guide. IEEE J. Quantum Electron. **23**(5), 510–524 (1987)
32. Gordon, J.P.: Theory of the soliton self-frequency shift. Opt. Lett. **11**(10), 662–664 (1986)
33. Mitschke, F.M., Mollenauer, L.F.: Discovery of the soliton self-frequency shift. Opt. Lett. **11**(10), 659–661 (1986)
34. Özisik, M., Seçer, A., Bayram, M.: On solitary wave solutions for the extended nonlinear Schrödinger equation via the modifed F-expansion method (2023)
35. Borich, M.A., Smagin, V.V., Tankeev, A.P.: Stationary states of extended nonlinear Schrödinger equation with a source. Phys. Met. Metallogr. **103**, 118–130 (2007)
36. Su, D., Yong, X., Tian, Y., Tian, J.: Breather and rogue wave solutions of an extended nonlinear Schrödinger equation with higher-order odd and even terms. Mod. Phys. Lett. B **32**(26), 1850309 (2018)
37. Monisha, S., Priya, V.N., Senthilvelan, M., Rajasekar, S.: Higher order smooth positron and breather positron solutions of an extended nonlinear Schrodinger equation with the cubic and quartic nonlinearity. Chaos Solitons Fractals **162**, 112433 (2022)
38. Sedletsky, Y.V., Gandzha, I.S.: Hamiltonian form of an Extended Nonlinear Schrödinger Equation for Modelling the Wave field in a System with Quadratic and Cubic Nonlinearities. Math. Model. Nat. Phenom. **17** (2022)
39. Crabb, M., Akhmediev, N.: Two-breather solutions for the class I infinitely extended nonlinear Schrödinger equation and their special cases. Nonlinear Dyn. **98**, 245–255 (2019)
40. Huang, Y., Jing, H., Li, M., Ye, Z., Yao, Y.: On solutions of an extended nonlocal nonlinear Schrödinger equation in plasmas. Mathematics **8**(7), 1099 (2020)
41. Lou, Y., Zhang, Y., Ye, R.: Interactional solutions of the extended nonlinear Schrödinger equation with higher-order operators. Int. J. Comput. Math. **99**(10), 1989–2000 (2022)
42. Benedicks, M., Carleson, L.: The dynamics of the Hénon map. Ann. Math., 73–169 (1991)
43. Wang, X., Guan, N.: 2D sine-logistic-tent-coupling map for image encryption. J. Ambient Intell. Humaniz. Comput. **14**(10), 13399–13419 (2023)
44. Yuan, H.-M., Liu, Y., Gong, L.-H., Wang, J.: A new image cryptosystem based on 2D hyper-chaotic system. Multimed. Tools Appl. **76**, 8087–8108 (2017)
45. Mu, D., Xu, C., Liu, Z., Pang, Y.: Further insight into bifurcation and hybrid control tactics of a chlorine dioxide-iodine-malonic acid chemical reaction model incorporating delays. MATCH Commun. Math. Comput. Chem. **89**(3), 529–566 (2023)
46. Li, P., Peng, X., Xu, C., Han, L., Shi, S.: Novel extended mixed controller design for bifurcation control of fractional-order Myc/E2F/miR-17-92 network model concerning delay. Math. Methods Appl. Sci. (2023). https://doi.org/10.1002/mma.9597
47. Xu, C., Liu, Z., Li, P., Yan, J., Yao, L.: Bifurcation mechanism for fractional-order three-triangle multi-delayed neural networks. Neural Process. Lett. **55**, 6125–6151 (2023). https://doi.org/10.1007/s11063-022-11130-y
48. Wang, P., Yin, F., ur Rahman, M., Khan, M.A., Baleanu, D.: Unveiling complexity: exploring chaos and solitons in modified nonlinear Schrödinger equation. Results Phys., 107268 (2023)
49. Pan, J., ur Rahman, M.: Breather-like, singular, periodic, interaction of singular and periodic solitons, and a-periodic solitons of third-order nonlinear Schrödinger equation with an efficient algorithm. Eur. Phys. J. Plus **138**(10), 1–12 (2023)

Publisher's Note